

Morphologically-Aware Consensus Computation via Heuristics-based IterATive Optimization (MACCHlatO)

Dimitri Hamzaoui <https://orcid.org/0000-0003-2775-8594>

Université Côte d’Azur, Inria, Epione Team, Sophia Antipolis, France

Sarah Montagne

Academic Department of Radiology, Hôpital Pitié-Salpêtrière, Assistance Publique des Hôpitaux de Paris, Paris, France

GRC 5 Predictive Onco-Urology, Sorbonne University, Paris, France

Raphaële Renard-Penna

Academic Department of Radiology, Hôpital Pitié-Salpêtrière, Assistance Publique des Hôpitaux de Paris, Paris, France

GRC 5 Predictive Onco-Urology, Sorbonne University, Paris, France

Nicholas Ayache

Université Côte d’Azur, Inria, Epione Team, Sophia Antipolis, France

Hervé Delingette <https://orcid.org/0000-0001-6050-5949>

Université Côte d’Azur, Inria, Epione Team, Sophia Antipolis, France

Abstract

The extraction of consensus segmentations from several binary or probabilistic masks is important to solve various tasks such as the analysis of inter-rater variability or the fusion of several neural network outputs. One of the most widely used methods to obtain such a consensus segmentation is the STAPLE algorithm. In this paper, we first demonstrate that the output of that algorithm is heavily impacted by the background size of images and the choice of the prior. We then propose a new method to construct a binary or a probabilistic consensus segmentation based on the Fréchet means of carefully chosen distances which makes it totally independent of the image background size. We provide a heuristic approach to optimize this criterion such that a voxel’s class is fully determined by its voxel-wise distance to the different masks, the connected component it belongs to and the group of raters who segmented it. We compared extensively our method on several datasets with the STAPLE method and the naive segmentation averaging method, showing that it leads to binary consensus masks of intermediate size between Majority Voting and STAPLE and to different posterior probabilities than Mask Averaging and STAPLE methods. Our code is available at <https://gitlab.inria.fr/dhamzaou/jaccardmap>.

Keywords: Consensus, Distance, Heuristics, Optimization, STAPLE

1. Introduction

The fusion of several segmentations into a single consensus segmentation is a classical problem in the field of medical image analysis related to the need to merge multiple segmentations provided by several clinicians into a single “consensus” segmentation. This problem has been recently revived by the development of deep learning and the multiplication of ensemble methods based on neural networks (Isensee et al., 2021). One of the most well-known methods to obtain a consensus segmentation is the STAPLE algorithm (Warfield

et al., 2004), where an Expectation-Maximization algorithm is used to jointly construct a consensus segmentation, and to estimate the raters’ performances posed in terms of sensitivities and specificities. The seminal STAPLE method (Warfield et al., 2004) creating a probabilistic consensus from a set of binary segmentations was followed by several follow-up works. For instance, Asman and Landman (2012) replaced global indices of performance by spatially dependent performance fields and Commowick et al. (2012) combined STAPLE with a sliding window approach to allow spatial variations of rater performances. Another improvement consisted in introducing the original image intensity information (Asman and Landman, 2013). Several alternatives to STAPLE were proposed, with a large diversity of approaches. Some of them decided to use a generative model but with different properties. For example, Audelan et al. (2020) modeled raters’ input maps by heavy-tailed distributions whose parameters are estimated by variational calculus, and Sabuncu et al. (2010) presented a model using a random field learnt on the whole set to model the interaction between the intensity maps and the corresponding label maps. Methods based on deep learning were also conceived, as in Zhang et al. (2020) where two CNNs are trained together to estimate simultaneously the consensus segmentation and each rater’s performance via an estimation of their spatial confusion matrices. Also in Ji et al. (2021) authors incorporate the expertise level of each rater and specific modules to better take into account disagreements between raters. However, those methods do not lead to explainable results and they require the collection of a preliminary training data on a consequent number of cases which make them not suitable on small datasets. In addition to those complex methods, several studies (Rohlfing and Maurer, 2007; Aljabar et al., 2009) show that simple majority voting (MV) could remain a suitable pick. However STAPLE and its simple yet robust probabilistic model remains the go-to method for consensus segmentation estimation (Warfield et al., 2004; Dewalle-Vignion et al., 2015) despite suffering from several limitations, some of them already addressed in the literature (Asman and Landman, 2012; Commowick et al., 2012; Asman and Landman, 2013) and some, to the best of our knowledge, never raised before.

In this article, we first analytically characterize the dependence of the STAPLE algorithm on the size of the background image and the choice of prior consensus probability. We then introduce an alternative consensus segmentation method, coined MACCHIato, which is based on the minimization of the squared distance between each binary segmentation and the consensus. After choosing a distance between binary or probabilistic shapes, the consensus is thus posed as the estimation of the Fréchet mean of this distance (an extension of centroids to metric spaces), which is independent of the size of the background image for a well-chosen distance. We show that the adoption of specific heuristics based on morphological distances (i.e. voxel-wise distances to the different binary masks based on morphological operations) during the optimization allows to provide a novel binary or probabilistic globally consistent consensus method that creates masks of intermediate size between Majority Voting and the STAPLE methods.

This work extends our MICCAI-UNSURE 2022 paper (Hamzaoui et al., 2022) by (1) Adding the Dice coefficient and its soft surrogates as distances between binary sets (2) Providing more mathematical details on baseline models and the STAPLE’s dependence on the background size and prior choice (3) Adding experiments and a dataset to justify the choice of selected heuristics and to analyze the impact on the consensus volume and

computational time and (4) Expanding the discussion in various ways including detailing the limitations of the proposed approach.

2. Estimation of a soft or hard consensus from binary segmentations

In the remainder, we consider the problem of generating a consensus segmentation T_n , $1 \leq n \leq N$ given K binary segmentations $\mathcal{S} = \{S^1, \dots, S^K\}$, $S_n^k \in \{0, 1\}$ of size N provided by each rater k . The consensus segmentation may be either a *hard* binary segmentation $T_n \in \{0, 1\}$ or a *soft* probabilistic segmentation $\tilde{T}_n \in [0, 1]$, the tilde sign indicating that we are dealing with a continuous probabilistic consensus value, rather than a binary one. Given a soft consensus, one can easily generate a hard consensus by thresholding the soft consensus voxels at the 0.5 limit. Yet, this raises the issue of dealing with voxels that are exactly at the 0.5 value which can be either set arbitrarily to one of the 2 classes or set aside to a third class.

In terms of probabilistic framework, the main approach is to consider that each observed binary segmentation S^k results from a random process applied on a consensus segmentation T which is captured by the likelihood distribution $p(S^k|T, \theta_k)$ also involving some parameters θ_k specific to each rater k . A prior probability on the consensus $p(T)$ is also defined related to the general *a priori* knowledge about the consensus segmentation. Then a hard consensus can be obtained as a maximum likelihood $T = \arg \max_M p(\mathcal{S}|M)$ or maximum *a posteriori* estimate $U = \arg \max_U p(\mathcal{S}|U)p(U)$ whereas a soft consensus is obtained as the posterior probability $p(\tilde{T}|\mathcal{S}) = p(\mathcal{S}|\tilde{T})p(\tilde{T})/p(\mathcal{S})$. The parameters θ_k are also estimated by maximum likelihood for hard consensus or maximum marginal likelihood for soft ones.

We make use of the following notations : FP_k , TP_k , FN_k , and TN_k are respectively the number of false positives, true positives, false negatives, and true negatives between observed mask S^k and consensus T , i.e. $FP_k = \sum_{n=1}^N S_n^k \wedge T_n$.

We consider as baseline methods to create a hard consensus the majority voting (MV) and the ML STAPLE (Maximum Likelihood STAPLE, a binary version of STAPLE) algorithms whereas mask averaging (MA) and STAPLE algorithm are baseline approaches for the soft consensus estimation. We describe below the hypotheses in terms of probability distribution associated with those baseline models and discuss their limitations.

2.1 Majority Voting and Mask Averaging Models

We first make the hypothesis of voxel independence, i.e. that the binary value of each voxel of an observed segmentation mask S^k is independent of the values of other voxels : $p(S^k|T) = \prod_{n=1}^N p(S_n^k|T_n)$. Furthermore, we consider that the prior and likelihood probability are simple Bernoulli distributions of the same parameter $b_n \in [0, 1]$: $p(S_n^k = 1|b_n) = p(T_n = 1|b_n) = b_n$. This means that the probability parameter b_n is potentially different for all voxels, but the same for all raters : $\theta_k = \theta = \{b_n\}$. Also, the observed masks \mathcal{S} do not directly depend on the consensus but share the same distribution.

Therefore the likelihood of observing the whole segmentation data is then

$$p(\mathcal{S}|\theta) = \prod_{k=1}^K \prod_{n=1}^N b_n^{S_n^k} (1 - b_n)^{1-S_n^k} = \prod_{n=1}^N b_n^{S_n^+} (1 - b_n)^{S_n^-}$$

where S_n^+ (resp. $S_n^- = K - S_n^+$) is the number of times voxel n is equal to 1 (resp. 0) in the observed segmentation masks $S^k, 1 \leq k \leq K$. After maximizing the likelihood, one trivially gets the Bernoulli parameter as $p(S_n^k = 1|b_n) = p(T_n = 1|b_n) = \frac{S_n^+}{K} = b_n$, leading to the Mask Averaging consensus formula where the probability of having a foreground voxel is the frequency of positive voxels in the observed masks S^k . To estimate the hard consensus, one needs to maximize $p(T_n|b_n)$ thus leading to majority voting : $T_n = 1$ if $S_n^+ > S_n^-$ and $T_n = 0$ if $S_n^+ < S_n^-$.

Limitations Majority voting and mask averaging are simple and easy-to-understand mechanisms to choose a consensus. Yet they suffer from the fact that this decision is purely local without any influence from the neighboring pixels. This can lead to situations where the hard consensus includes some isolated voxels or has very irregular boundaries. This is especially true for mask averaging, which does not have any mechanisms to enforce inter-rater consistency and that relies on the implicit assumption that the neighboring voxels of a segmented voxel are likely to be segmented, which is not the case on the boundaries. Another limitation of majority voting is the case where the number of raters K is even and therefore many decisions are ambiguous with as many foreground than background voxels. Finally, those simple models assume that all raters' contributions to the consensus are equal which may not be the case. In particular, an underperforming rater will bias the soft consensus with mask averaging.

2.2 STAPLE model

In the STAPLE algorithm (Warfield et al., 2004), all voxels are also assumed independent but the probability that S_n^k is equal to T_n depends on whether T_n is a background or foreground voxel, and on the rater k . More precisely, $p(S_n^k = T_n|T_n = 1) = p_k$ and $p(S_n^k = T_n|T_n = 0) = q_k$ where p_k is the sensitivity of rater k and q_k its specificity.

Prior Consensus The consensus prior probability is here supposed to factorize as the product of voxel priors w_n values $p(T) = \prod_{n=1}^N P(T_n) = \prod_{n=1}^N w_n$. The original STAPLE paper (Warfield et al., 2004) also introduced an Ising Markov random field model as a prior consensus probability to enforce that a voxel prior value depends on that of its neighbors. However, this approach leads to solving iteratively graph cuts problems and is not available in most widely used STAPLE implementations. Instead, the original paper assumes simple independent priors that lead to closed-form updates. Choosing $w_n = w = \frac{1}{2}$ is a non-informative prior but another common choice is to have a spatially uniform value $w_n = w = \frac{1}{NK} \sum_{n,k} S_n^k$ which is the average relative size of the foreground object in the observed segmentation masks. We further consider more general priors of the form $w = \frac{A}{N^\alpha}$, with A a constant independent of the image size, and $\alpha \in \mathbb{N}$ an exponent. The non-informative case $w_n = 0.5$ corresponds to $\alpha = 0$ while the average object size to $\alpha = 1$.

Maximum likelihood STAPLE (ML STAPLE) The likelihood of the observed data simply writes as $\mathcal{L}(T, \theta) = \prod_{k=1}^K p_k^{\text{TP}_k} (1 - p_k)^{\text{FN}_k} q_k^{\text{TN}_k} (1 - q_k)^{\text{FP}_k}$ and does not involve the prior on the consensus. There is no closed-form expression for the estimation of the rater parameters (p_k, q_k) and the hard consensus (T) maximizing the likelihood. But an iterative maximization of the likelihood is possible by setting its derivatives to zero which leads to the update equation :

$$p_k = \frac{\text{TP}_k}{\text{TP}_k + \text{FN}_k} \quad q_k = \frac{\text{TN}_k}{\text{TN}_k + \text{FP}_k} \quad (1)$$

$$s_n^+ = \prod_{k=1}^K p_k^{S_n^k} (1 - p_k)^{1-S_n^k} \quad s_n^- = \prod_{k=1}^K q_k^{1-S_n^k} (1 - q_k)^{S_n^k} \quad (2)$$

$$T_n = 1 \text{ if } s_n^+ > s_n^- \quad T_n = 0 \text{ if } s_n^+ < s_n^-$$

Maximum marginal likelihood (MML STAPLE) The *marginal likelihood* or *evidence* writes as $p(\mathcal{S}|\theta) = \prod_{n=1}^N (w_n \prod_k p_k^{S_n^k} (1 - p_k)^{1-S_n^k} + (1 - w_n) \prod_k q_k^{1-S_n^k} (1 - q_k)^{S_n^k})$ and is only a function of the rater parameters θ_k . Its maximization is not tractable in closed form but the expectation-maximization algorithm provides a way to estimate some local maxima. The E-step consists in evaluating the posterior probability from Bayes law with the current estimated sensitivities and specificities :

$$u_n = p(\tilde{T}|\theta, \mathcal{S}) = \frac{w_n \prod_k p_k^{S_n^k} (1 - p_k)^{1-S_n^k}}{w_n \prod_k p_k^{S_n^k} (1 - p_k)^{1-S_n^k} + (1 - w_n) \prod_k q_k^{1-S_n^k} (1 - q_k)^{S_n^k}} \quad (3)$$

The M-step updates the parameters p_k and q_k as follows :

$$p_k = \frac{\sum_{n, S_n^k=1} u_n}{\sum_n u_n} = \frac{\text{sTP}_k}{\text{sFN}_k + \text{sTP}_k} \quad q_k = \frac{\sum_{n, S_n^k=0} (1 - u_n)}{\sum_n (1 - u_n)} = \frac{\text{sTN}_k}{\text{sTN}_k + \text{sFP}_k} \quad (4)$$

where sTP_k , sTN_k , sFP_k , sFN_k are the "soft extension" of the number of true positive, true negative, false positive, and false negative voxels from rater k .

2.2.1 INFLUENCE OF THE PRIOR TERM

We can better understand the influence of the prior when estimating the probability to belong to a consensus by writing its logit $\text{logit}(u_n) = \ln\left(\frac{u_n}{1-u_n}\right)$ from Eq.3 :

$$\text{logit}(u_n) = \text{logit}(w_n) + \sum_{k, S_n^k=1} \log\left(\frac{p_k}{1-q_k}\right) + \sum_{k, S_n^k=0} \log\left(\frac{1-p_k}{q_k}\right) \quad (5)$$

Thus, we see that to estimate u_n each foreground voxel of rater k "votes" with a (usually) positive quantity $\log\left(\frac{p_k}{1-q_k}\right)$ whereas each background voxel "votes" with a (usually) negative quantity $\log\left(\frac{1-p_k}{q_k}\right)$. Then the prior term $\text{logit}(w_n)$ biases this vote depending on whether w_n is greater or smaller than $\frac{1}{2}$.

2.2.2 INFLUENCE OF THE BACKGROUND SIZE

In many cases, the size N of images that contain the objects delineated by the raters is arbitrary since it can be the size of the original image (with a large value of N) or the size of a restricted region of interest (with a small value of N). It is therefore important to estimate the influence of the background size, i.e. the number of true negative voxels TN_k , in the estimation of the hard and soft consensus.

Influence on hard consensus Based on Eqs.1 and 2, the sensitivity and coefficient s_n^+ are not influenced by TN_k , but the specificities are. More precisely, we have $q_k = 1 - \frac{FP_k}{TN_k} + O((TN_k)^{-2})$, and therefore the quantity s_n^- tends towards 0 when TN_k reaches large values. This implies that the hard consensus converges towards the union of all observed segmentation masks when the background size becomes large.

Influence on soft consensus The posterior probability u_n and specificities q_k are mainly impacted by the increase of the background size, while the sensitivities are more marginally influenced. The nature of the soft consensus depends on the α exponent of the prior expression $w_n = \frac{A}{N^\alpha}$, and in particular we have :

$$\text{logit}(u_n) = \left(\sum_{k=1}^K S_n^k - \alpha \right) \log N + \log A + \ln \left(\frac{p_k}{sFP_k} \right) + \sum_{k, S_n^k=0} \ln(1 - p_k) + O(N^{-2})$$

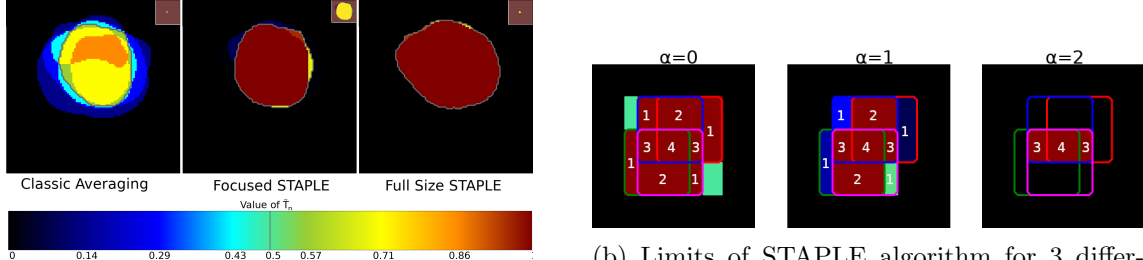
A direct consequence of this formula is that the background size impacts the obtained consensus, as can be seen in Fig. 1a where the consensus obtained when applying STAPLE on a bounding box tightly surrounding the organ (referred to as *Focused STAPLE* in Fig. 1a) appears as smaller and with more non-binary values than the one computed on the whole image (referred to as *Full size STAPLE* in Fig. 1a). Comparisons between STAPLE computed on both volumes are available in Tab. 10 in the appendices. Moreover, as seen in Fig.1b, the soft consensus when having a large background size depends on the value of α , with larger α corresponding to smaller consensus. The detailed proof is presented in Appendix A.

Removing the Influence of the background size We explore under which conditions the STAPLE model leads to consensus estimations that are independent of the background size. A first simplification of the model is to assume that all raters perform equally $p_k = p$, $q_k = q$. In this case, the global specificity maximizing the likelihood is $q = \frac{\sum_{k=1}^K TN_k}{\sum_{k=1}^K TN_k + FP_k}$ which is still dependent on the size of the background through TN_k .

A second simplification is to consider that each rater sensitivity and specificity are equal, i.e. $p_k = q_k = \gamma_k$. This implies that the rater performance is independent of the fact the consensus voxel is in the background or foreground. In this case, the parameter $p_k = q_k = \gamma_k$ can be interpreted as the accuracy parameter and its optimization leads to $\gamma_k = \frac{TP_k + TN_k}{N}$. It is easy to see that in that case, $\frac{s_n^+}{s_n^-} = \left(\frac{\gamma_k}{1-\gamma_k} \right)^{S_n^+ - S_n^-}$, and therefore the maximum likelihood is equivalent to majority voting when $\gamma_k > \frac{1}{2}$ which is independent of background size. With this simplification, and from Eq.5, the soft consensus obtained by maximizing the marginal likelihood with a non-informative prior $w_n = \frac{1}{2}$, is such that $\text{logit}(u_n) = (S_n^+ - S_n^-) \text{logit}(\gamma_k)$. The value of γ_k depends on the background size, but whether a voxel is more likely to be a background pixel $u_n > \frac{1}{2}$ does not depend on the background size.

2.2.3 LIMITATIONS

The STAPLE algorithm addresses the problem of taking into account the performance of raters when building a consensus segmentation. However, this approach has the drawback



(a) Impact of background size on a simple 2D case with 7 raters (the 7th is an empty map), with STAPLE computed on a 67×61 image (middle), and 640×640 (right) with $w = (\sum_{n,k} S_n^k)/NK$. The relative size of the structure can be seen at the top right corner.

(b) Limits of STAPLE algorithm for 3 different values of α on a toy example with 4 raters providing the red, blue, green and magenta contours. The figures are the number of raters who segmented this zone, and the colors are the probability of the soft consensus with colormap borrowed from Fig.1a.

Figure 1: Impact of STAPLE hyperparameters and background size on the soft consensus

of being dependent on the choice of the prior, and the background size. This dependence of the STAPLE consensus can be explained by the fact that it is a generative model which should explain the foreground and the background voxels separately. When assuming that the rater performance is the same in both background and foreground, then the model becomes equivalent to majority voting. This dependence is a subject of concern as STAPLE is often used as a standard in label fusion works. To improve the robustness of comparisons with novel methods and decrease the impact of this hidden hyperparameter, researchers may compute STAPLE consensus using several bounding boxes, or at least indicates the size of the bounding box on which STAPLE was applied.

The use of local sliding windows in STAPLE as in Commowick et al. (2012) can somewhat mitigate the background size effect, but smaller structures in images can still be impacted and the window size remains a hyperparameter which is difficult to set.

3. MACCHIAtO framework

3.1 Main approach description

In the previous section, we have seen that only the majority voting and mask averaging algorithms lead to a consensus that is independent of the background size. Yet, those algorithms are purely local at the voxel level and can lead to irregular boundaries or isolated voxels.

In this section we introduce a new framework to compute soft and hard consensus that are i) invariant from the background size and ii) dependent on the global morphology of each binary object. This approach is coined MACCHIAtO for Morphologically-Aware Consensus Computation via Heuristics-based IterATIVE Optimization.

Distance-based approach We formulate the estimation of a hard consensus T as the minimization of the sum of the square distance between the consensus T and each observed

binary mask S^k :

$$T = \arg \min_{M \in \{0,1\}^N} \sum_{k=1}^K d(M, S^k)^2 \quad (6)$$

where $d(T, S^k)$ is a distance as defined in Deza and Deza (2016) between the two masks S^k and T . This is equivalent to estimating the consensus as a maximum likelihood where the likelihood can be written as $p(S^k|T) \propto \exp(-\lambda d(T, S^k)^2)$. We can note that the squared sum $\sum_{k=1}^K d(M, S^k)^2$ also corresponds to the definition of a Fréchet variance. Based on this interpretation, T appears as the Fréchet mean of \mathcal{S} i.e. its centroid in the metric space defined by d .

Link with baseline models In section 2.2.2, we have seen that when the sensitivity and specificity are equal, the maximization of the STAPLE model leads to the majority voting algorithm. In this case, we can write the likelihood $p(S^k|T) = \gamma_k^{\text{TP}_k + \text{TN}_k} (1 - \gamma_k)^{\text{FP}_k + \text{FN}_k}$ (where γ_k is the accuracy parameter) which is a product of N independent Bernoulli distributions. Since the Bernoulli distribution is a member of the exponential family (Dai et al., 2013), it can be also written as $p(S^k|T) \propto \exp(-\lambda_k (\text{FP}_k + \text{FN}_k))$ where $\lambda_k = \text{logit}(\gamma_k)$. The number of false positives or false negatives $\text{FP}_k + \text{FN}_k$ is the number of elements of symmetric difference between the two sets S^k and T : $\text{FP}_k + \text{FN}_k = |T \Delta S^k| = |(T \cup S^k) \setminus (T \cap S^k)|$ and is also called the *Hamming distance* in information theory. Thus, by choosing $d(T, S^k) = \sqrt{|T \Delta S^k|}$, the maximum likelihood leads to majority voting consensus (as detailed in Appendix B).

Soft consensus framework On the baseline models, soft consensus were obtained as posterior probabilities of having a consensus from the observed binary masks. However, from the likelihoods $p(S^k|\tilde{T}) \propto \exp(-\lambda d(\tilde{T}, S^k)^2)$, the computation of the posterior $p(\tilde{T}|\mathcal{S})$ may not be tractable due to the difficulty of computing the normalization constant. Instead, we propose to approximate $p(\tilde{T}_n|\mathcal{S})$ by the quantity $\tilde{U}_n \in [0, 1]$ such that $\tilde{U} \in [0, 1]^N$ minimizes the quantity :

$$\tilde{U} = \arg \min_{\tilde{X} \in [0,1]^N} \sum_{k=1}^K d^s(\tilde{X}, S^k)^2 \quad (7)$$

where $d^s(\tilde{X}, S^k)$ is a distance between the probabilistic array \tilde{X} and the binary mask S^k . More precisely, the distances $d^s(\tilde{X}, S^k)$ considered are *soft surrogate* of the distance between binary sets $d(\tilde{X}, S^k)$ such that $d^s(\tilde{X}, S^k)^2 = d(\tilde{X}, S^k)^2$ when $\tilde{X} \in \{0, 1\}^N$. For instance, the distance $d(\tilde{X}, S^k) = \|\tilde{X} - S^k\|$ is a soft surrogate of the Hamming distance since $|\tilde{X} \Delta S^k| = \|\tilde{X} - S^k\|^2$. Besides it is clear that the mask averaging (MA) method is a soft consensus minimizing the following squared sum $\sum_{k=1}^K \|\tilde{U} - S^k\|^2$.

Optimization approach The estimation of the soft and hard consensus is independent of the background size if the distance $d(T, S^k)$ is invariant to the number of true negatives. Besides, unlike the MV and MA algorithms, the optimization cannot be performed at the voxel level when the distance cannot be split voxelwise. Instead of optimizing the whole foreground object, we chose to consider each connected component separately from each other to obtain more coherent results. Finally, we further split the optimization into subcrowns with various heuristics to speed up the computation.

3.2 Distances between binary masks

We detail below the selected distances between binary sets that are considered and their associated soft surrogates. We mainly focus on distances based on two widely used methods to measure the overlap between binary segmentations : the Jaccard and Dice coefficients.

Jaccard distance The Jaccard coefficient (aka IoU) between binary masks A and $B \in \{0, 1\}^N$ is defined as : $\text{Jac}(A, B) = \frac{|A \cap B|}{|A \cup B|}$. In Kosub (2019), it is shown that its complementary to 1 $\text{dist}_J(A, B) = 1 - \text{Jac}(A, B) = \frac{|A \Delta B|}{|A \cup B|}$ is a metric between binary sets following the triangular inequality. Several formulations of soft surrogates exist that extend the Jaccard distance. We focused specifically on two of them : the Soergel metric (Späth, 1981; Deza and Deza, 2016) $d_{\text{Sg}}(x, y) = \frac{\sum_i \max(x_i, y_i) - \min(x_i, y_i)}{\sum_i \max(x_i, y_i)}$ which follows the triangular inequality but is not differentiable, and the widely-used Tanimoto distance (Willett et al., 1998; Deza and Deza, 2016; Leach and Gillet, 2007) $d_{\text{Tan}}(x, y) = 1 - \frac{\sum_i x_i y_i}{\sum_i x_i^2 + y_i^2 - x_i y_i} = \frac{\|x - y\|^2}{\|x - y\|^2 + \langle x, y \rangle}$.

Dice coefficient It is defined as $\text{DSC}(A, B) = \frac{2|A \cap B|}{|A| + |B|}$ and is widely used in image segmentation as a performance index. Indeed, the Dice index is equal to the F1-score and corresponds to the harmonic mean of the sensitivity and positive predictive value. It is closely related to the Jaccard coefficient as $\text{DSC}(A, B) = \frac{2\text{Jac}(A, B)}{1 + \text{Jac}(A, B)}$. The Dice distance $\text{dist}_D(A, B) = 1 - \text{DSC}(A, B)$ is a near-metric i.e. it respects a relaxed form of the triangular inequality (Gragera and Suppakitpaisarn, 2018). Soft surrogates of the Dice distance have been developed especially as a loss function in deep learning. We consider in the remainder two main extensions of the Dice distance (Ma et al., 2021) on non-binary sets defined as $d_{\text{pSD}}(x, y) = 1 - \frac{2\sum_i x_i y_i}{\sum_i x_i^p + \sum_i y_i^p}$ where $p \in \{1, 2\}$.

By construction, all those distances only depend on segmented pixels and are independent of the background size. Note that both distances are extended to get a null distance between two empty sets. Using those distances in the Fréchet variance computation, the inclusion of voxels segmented by a large number of raters (resp. a few raters) decreases (resp. increases) its value. The different formulations of the MACCHIAtO framework are summarized in table 1.

Table 1: Distances between binary sets and their soft surrogate considered to compute hard and soft consensus with the MACCHIAtO framework

Hard Consensus Method	Soft Consensus Method	Distance	Soft Surrogate	Computation-level
Majority Voting	Mask Averaging	$ A \Delta B $	$\ x - y\ $	Voxel-level
ML STAPLE	MML STAPLE	NA	NA	Image-level
MACCHIAtO-J	MACCHIAtO-TJ	Jaccard d_J	Tanimoto d_{Tan}	Connected component level
	MACCHIAtO-SJ		Soergel d_{Sg}	
MACCHIAtO-D	MACCHIAtO-1SD	Dice d_D	$d_{1\text{SD}}$	
	MACCHIAtO-2SD		$d_{2\text{SD}}$	

3.3 Heuristic computation based on morphological distance and crowns

Domain of optimization Since the distances listed in the previous section are independent of the number of true negatives, their computations can be restricted to the union of all rater masks : $\mathcal{E}_S = \{n | \sum_{k=1}^K S_n^k > 0\}$. Furthermore, we consider that to decide whether a voxel belongs to the consensus, one should only take into account the regional context associated with the connected components surrounding that voxel, since far-away components may not be relevant. Therefore, we choose to minimize separately the Fréchet variances of Eqs. 6 and 7 for each connected component St of the masks union \mathcal{E}_S . Therefore, in practice, we minimize the *Local Mean Squared Distance* between \mathcal{S} and the consensus : $\text{LMSD}_d(\mathcal{S}, M) = \sum_{St \subset \mathcal{E}_S} \frac{1}{K} \sum_k d(S_{\parallel St}^k, M_{\parallel St})^2$ where $S_{\parallel St}^k$ (resp. $M_{\parallel St}$) are the restriction of the binary masks S^k (resp. M) to the connected component St . A benefit of this choice is that the determination of the Fréchet Mean behaves similarly to a structure-wise MV, as the Fréchet Mean of components segmented by less than half of the raters is the null set. However, contrary to MV, raters who do not segment a component kept by the majority of raters do not bias its consensus segmentation, as their contribution to the associated LMSD is $\frac{1}{K} \delta_\emptyset(M_{\parallel St}) = 0$ and does not impact the Fréchet mean. To lighten notations, we drop the St index in the remainder. It is equivalent to considering that \mathcal{E}_S has only one single connected component.

Subcrown-based optimization The minimization of the Fréchet variance is a combinatorial problem with a complexity of $2^{|\mathcal{E}_S|}$ for the naive approach. Furthermore, it may lead to several global minima when the number of raters K is small. For those reasons, we propose instead to seek a local minimum of the Fréchet variance by introducing some heuristics in the optimization. With this approach, the local minimum has a lower complexity to compute and, by construction, is maximally connected to avoid isolated voxels.

More precisely, instead of a computationally expensive per voxel minimization of the Fréchet variance, we decompose the set \mathcal{E}_S into a set of *subcrowns* that take into account the global morphological relationships between each rater mask. The formal definition of subcrowns requires the specification of distance maps $Dm_{\mathcal{N}}(S^k)$ to each binary mask S^k on \mathcal{E}_S according to a chosen neighborhood \mathcal{N} . This one can be either the 4 or 8 (resp. 6 or 26) connectivity in 2D (resp. 3D). The distance $Dm_{\mathcal{N}}(S^k)$ is set to 0 for all voxels inside the object S^k .

The global morphological distance map is the sum of those distance maps

$$D_S^{\mathcal{N}} = \sum_{S^k \in \mathcal{S}} Dm_{\mathcal{N}}(S^k)$$

for all raters on \mathcal{E}_S . A *crown* $C_{td}^{\mathcal{N}}$ is defined as the set of voxels having the same global morphological distance td . Those crowns realize a partition of \mathcal{E}_S ($\mathcal{E}_S = \coprod_{td} C_{td}^{\mathcal{N}}$), and the 0-crown corresponds by construction to the intersection of all masks in \mathcal{S} .

We further split each crown as a set of *subcrowns* by grouping the voxels that have been produced by the same set of raters. In other words, a subcrown corresponds to a set of voxels located at the same morphological distance from the intersection of all rater masks

and which have been segmented by the same group of raters, as seen in Fig. 2a. Formally, a subcrown is noted $(C_{td}^{\mathcal{N}})^g$ where the superscript g corresponds to a group of raters and subcrowns realize a partition of a crown :

$$C_{td}^{\mathcal{N}} = \coprod_{g \in \mathcal{P}(\llbracket 1, K \rrbracket)} (C_{td}^{\mathcal{N}})^g, \text{ with } (C_{td}^{\mathcal{N}})^g = \{n | n \in C_{td}^{\mathcal{N}} \ \& \ \forall k \ S_n^k = (k \in g)\} \quad (8)$$

where $\mathcal{P}(\llbracket 1, K \rrbracket)$ is the power set (i.e. the set of all subsets) of the first K integers.

The process for the construction of subcrowns is illustrated in Fig. 2a

3.4 Hard consensus algorithm

The optimization proceeds in a greedy fashion by iteratively removing or adding subcrowns to the current estimate of the consensus until the LMSD_d criterion stops decreasing. In Alg. 1, we use two concurrent strategies : either we start from the union of all masks and then remove subcrowns with decreasing distances (a strategy illustrated in Fig. 2b, or we start with the crown with the minimum distance and then add subcrowns of increasing distances. Both growing and shrinking strategies are applied as the greedy process can lead to different results, and we keep the consensus associated with the minimum LMSD_d of both strategies and the null set. The latter is also tested in the last stage since the distance of a set M to the null set is $\delta_{\emptyset}(M)$, for both Dice and Jaccard distances. This discontinuity is not compatible with the iterative process and calls for a independent test.

Examples of consensus obtained with this strategy can be seen in Fig. 3. Thus, the resulting consensus leads to a consistent grouping since all voxels belonging to the same connected component, having the same morphological distance, and being generated by the same group of raters will end up in the same class. Alternative optimization approaches could have been based on adding or removing single voxels (smaller than subcrowns) or crowns (larger than subcrowns). While voxel-based minimization would be very time-consuming, especially in 3D, conversely crown-based would lead to suboptimal results as crowns can be fairly large. Thus, the Morphologically-Aware Consensus Computation via Heuristics-based Iterative Optimization (MACCHIAtO) algorithm is designed to be a good compromise between computational efficiency and consistency, with a number of iterations exponentially depending on K but which is lower than the naive $2^{|\mathcal{E}_S|}$ complexity.

3.5 Soft consensus algorithm

The estimation of a probabilistic or soft consensus is based on the minimization of the sum of square surrogate distances as displayed in Eq. 7 and the optimization is split for each connected component of the mask union \mathcal{E}_S .

The *soft MACCHIAtO* algorithm extends the previous approach to minimize the criterion $\text{LMSD}_{ds}(\tilde{T}, \mathcal{S})$. A brute force approach would lead to the optimization of a sum of K rational polynomials over a set of $|\mathcal{E}_S|$ scalars. Instead, we proceed in a greedy manner, separately on each connected component of \mathcal{E}_S , by starting with the mean consensus and optimizing successively subcrowns of increasing distances. All subcrowns of increasing dis-

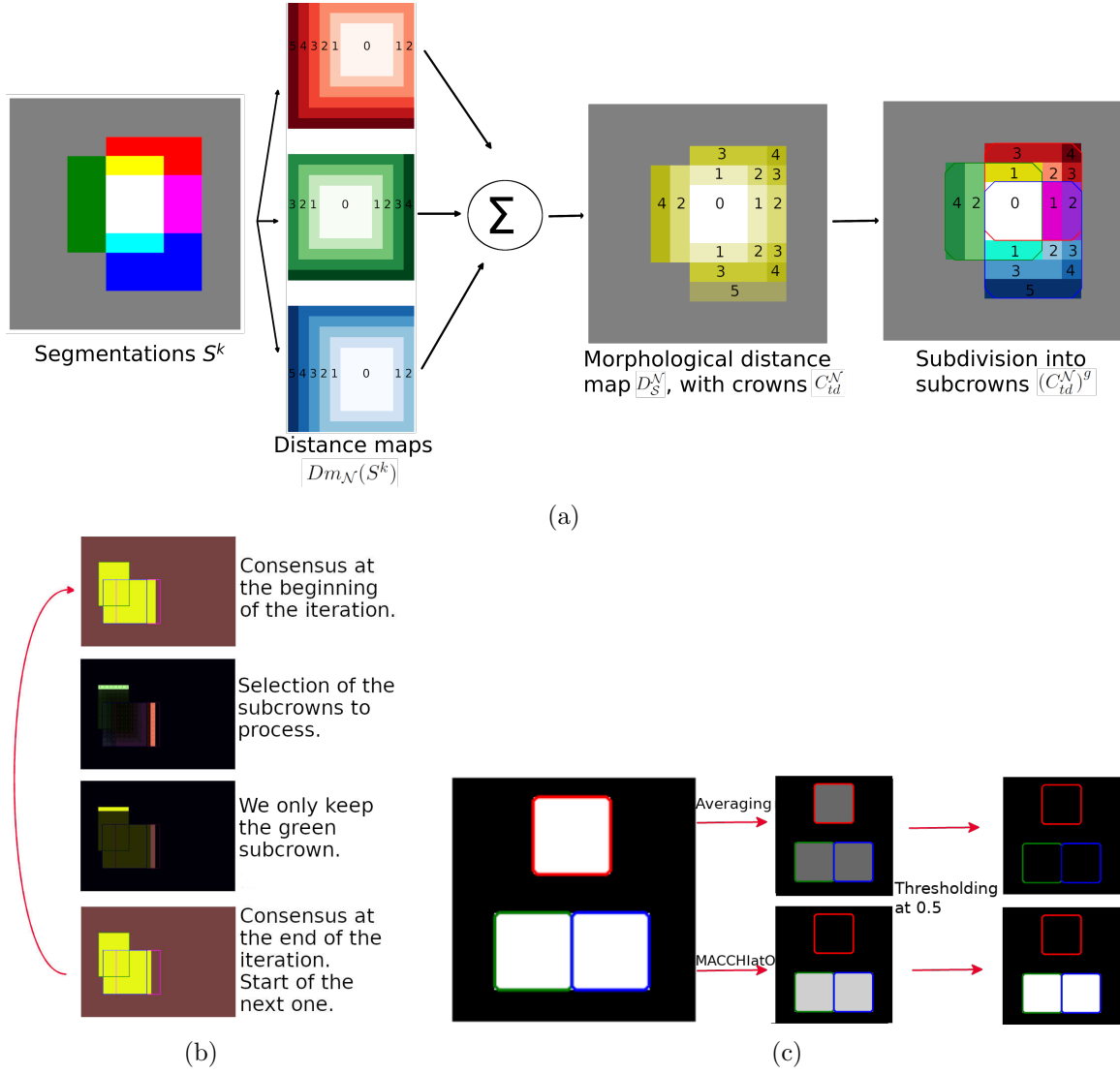


Figure 2: (a) Construction of the heuristics. From left to right: Segmentations by 3 raters (red, green, and blue); computation of the associated distance maps $Dm_N(S^k)$; merging into the morphological distance map D_S^N restricted to the voxels segmented at least one; subdivision into subcrowns (1 color = 1 subcrown) based on morphological distance and raters). (b) An iteration of the shrinking approach with the selection of sub-crowns and the evaluation of their contribution to the $LMSD_d$ (c) Application of mask averaging and soft MACCHIatO on a toy example with three segmentations (red, green, and blue contours). After thresholding, averaging gives an empty segmentation whereas the soft MACCHIatO method is more inclusive and outputs one connected component.

Input: \mathcal{S} segmentation maps, \mathcal{N} neighborhood, d distance
Result: T
Initialization: Computation of $D_{\mathcal{S}}^{\mathcal{N}}$, $td_u = \max(D_{\mathcal{S}}^{\mathcal{N}})$, $td_i = \min(D_{\mathcal{S}}^{\mathcal{N}})$;
 $T^u = \bigcup_k S^k$; $T^i = \{n | (D_{\mathcal{S}}^{\mathcal{N}})_n = td_i\}$
while $\text{LMSD}_d(T^u, \mathcal{S})$ decreases **do** // Shrinking strategy
 for $g \in \mathcal{P}(\llbracket 1, K \rrbracket)$ **do**
 if $\text{LMSD}_d((T^u / (C_{td_u}^{\mathcal{N}})^g), \mathcal{S}) < \text{LMSD}_d(T^u, \mathcal{S})$ **then**
 $T^u \leftarrow T^u / (C_{td_u}^{\mathcal{N}})^g$
 end
 end
 $td_u \leftarrow \max(\{x \in D_{\mathcal{S}}^{\mathcal{N}} | x < td_u\})$
end
while $\text{LMSD}_d(T^i, \mathcal{S})$ decreases **do** // Growing strategy
 for $g \in \mathcal{P}(\llbracket 1, K \rrbracket)$ **do**
 if $\text{LMSD}_d((T^i \cup (C_{td_i}^{\mathcal{N}})^g), \mathcal{S}) < \text{LMSD}_d(T^i, \mathcal{S})$ **then**
 $T^i \leftarrow T^i \cup (C_{td_i}^{\mathcal{N}})^g$
 end
 end
 $td_i \leftarrow \min(\{x \in D_{\mathcal{S}}^{\mathcal{N}} | x > td_i\})$
end
 $T \leftarrow \arg \min_{T \in \{T^u, T^i, \emptyset\}} \text{LMSD}_d(T, \mathcal{S})$

Algorithm 1: Hard consensus algorithm.

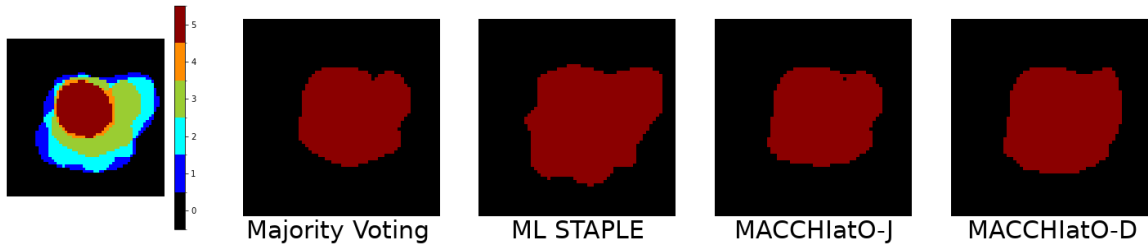


Figure 3: Comparison of several hard consensus methods on a 2D slice with 5 raters using MV, ML STAPLE and both hard MACCHIAtO. On the left is indicated the number of raters who segmented each pixel.

tances are iteratively considered until $\text{LMSD}_d(\tilde{T}, \mathcal{S})$ stops decreasing. For each subcrown $r = (C_{td}^{\mathcal{N}})^g$, we seek the scalar value $p_r \in [0, 1]$ such that it minimizes

$$p_r = \arg \min_{x \in [0,1]} (d(\tilde{T}_{(td,g),x}, \mathcal{S})), \text{ with } \tilde{T}_{(td,g),x} = \begin{cases} x & \text{if } n \in r \\ \tilde{T}_n & \text{otherwise} \end{cases}.$$

The algorithm is described in Alg.2 and iteratively optimizes each subcrown from the inside to the outside of the $\mathcal{E}_{\mathcal{S}}$ set. We have observed no gain in combining a growing and a shrinking exploration of subcrowns contrary to Alg. 1. For the optimization process of Eq. 3.5, we use the SLSQP algorithm (Kraft, 1988) implemented in Scipy v1.7.3 (Virtanen et al., 2020). Resulting consensus can be seen in Figs. 4, 6 and 7.

Input: \mathcal{S} segmentation maps, \mathcal{N} neighborhood, d^s distance

Result: \tilde{T}

Initialization: Computation of $D_{\mathcal{S}}^{\mathcal{N}}$; $\tilde{T} = \frac{1}{K} \sum_{k=1}^K S^k$

while $\text{LMSD}_{d^s}(\tilde{T}, \mathcal{S})$ decreases **do**

for $td \in D_{\mathcal{S}}^{\mathcal{N}}$ in increasing order **do**

for $g \in \mathcal{P}([1, K])$ **do**

$p = \arg \min_{x \in [0,1]} (\text{LMSD}_{d^s}(\tilde{T}_{(td,g),x}, \mathcal{S}))$ **with** $\tilde{T}_{(td,g),x} = \begin{cases} x & \text{on } (C_{td}^{\mathcal{N}})^g \\ \tilde{T} & \text{elsewhere} \end{cases}$

$\tilde{T} \leftarrow \tilde{T}_{(td,g),p}$

end

end

end

Algorithm 2: Soft consensus algorithm

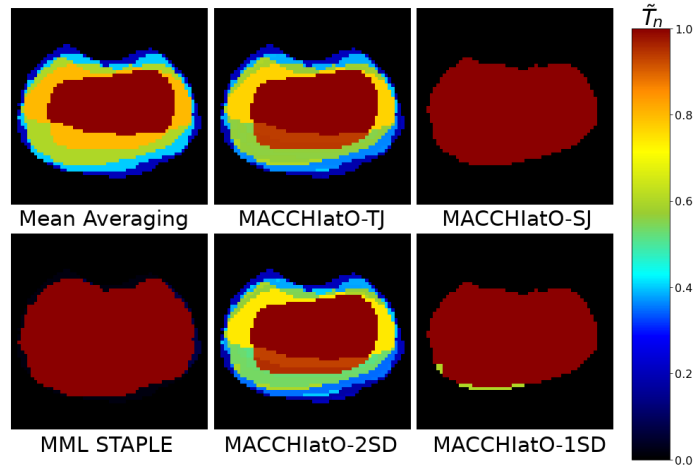


Figure 4: Comparison of several soft consensus methods on a 2D case with 5 raters using MA, STAPLE and MACCHIlatO with different distances.

4. Results

4.1 Datasets and Implementation Details

We tested our method on 3 datasets :

- A private database of transition zones of prostate T2w MR images, composed of 40 cases segmented by 5 raters.
- The publicly available MICCAI MSSEG 2016 dataset of Multiple Sclerosis lesions segmentations (Commowick et al., 2018) segmented from Brain MR images, with 15 subjects segmented by 7 raters
- The publicly available SCGM dataset (Prados et al., 2017), with 40 spinal cords and their grey matter segmented by 4 raters. We used the whole spinal cord segmentation (SCGM-SC) and the grey matter segmentation (SCGM-GM).

Images from the private dataset (resp. MSSEG dataset, SCGM dataset) have a size of $[80-288] \times [320-640] \times [320-640]$ voxels (resp. $[144-261] \times [224-512] \times [224-512]$ voxels and $[3-28] \times [100-655] \times [100-776]$ voxels). It was possible to extract from the private dataset bounding boxes of size $[58-227] \times [53-184] \times [62-180]$ voxels. Similarly, we were able to extract from SCGM-SC (resp. SCGM-GM) bounding boxes of size $[3-20] \times [15-90] \times [24-131]$ voxels (resp.) From the 3D private dataset, we created a 2D subset by extracting a single slice for each patient located at the base of the prostate since this region is subject to a high inter-rater variability (Becker et al., 2019; Montagne et al., 2021).

Examples for each dataset of segmentations by the different raters of the same case are available in Appendix C (Fig. 8).

Implementation details In the remainder, STAPLE results were produced by using the algorithm implemented in SimpleITK v2.0.2 (Lowekamp et al., 2013). All MACCHIAtO methods used the 8 or 26-connectivity neighborhood for 2D or 3D cases. MACCHIAtO code is available at <https://gitlab.inria.fr/dhamzaou/jaccardmap>

4.2 Heuristics relevance

In Section 3.3, we have presented the subcrown-based heuristics that drives the optimization of the local mean square distance criteria. Indeed, those subcrown group voxels are based on three properties : their morphological distance, the connected component they belong to, and the raters who segmented them. To check if this heuristics is appropriate, we compared it with two alternatives :

- The first alternative iteratively minimizes the LMSD_d at the crown level (as defined in subsection 3.3 and represented in Fig. 2a), without any rater-related property.
- The other one iteratively processes each voxel separately.

We compared the 3 heuristics by computing a soft consensus (with the Tanimoto distance) on the toy example of Fig. 5, and we display their optimized value of LMSD_{ds} and their computation time in Table 2. Furthermore, since the size of \mathcal{E}_S is small, we could estimate the true minimizer of LMSD_{ds} that involves the optimization of $|\mathcal{E}_S|$ parameters.

Table 2: Computed LMSD_{ds} and computation time for the soft consensus with Tanimoto distance on the toy example of Fig. 5 using three different heuristics and the true minimizer.

Heuristics	LMSD_d	Time
Subcrown-based heuristics	0.159	0.26s
Crown-based heuristics	0.176	0.07s
Voxel-based approach	0.159	0.92s
Estimated True minimizer	0.159	0.55s

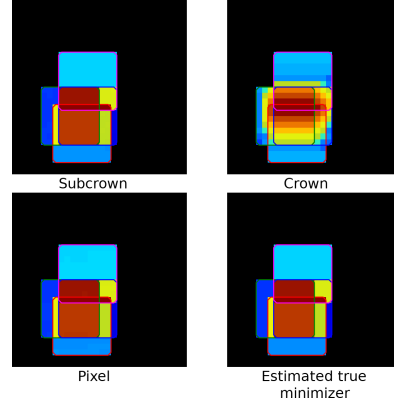


Figure 5: Different soft consensus obtained on a toy example. Each contour corresponds to one of the raters' segmentation and colors indicate the probability using the same colormap as Fig 4.

Unlike the crown-based heuristics, the subcrown-based and voxel-based heuristics appear to compute a consensus close to the real LMSD_{ds} minimizer. In addition, the subcrown method is significantly faster than the voxel-based approach.

We have also compared the three heuristics on two datasets in Table 3. The crown-based heuristics is the fastest method to compute but with the highest criteria LMSD_{ds} , whereas the voxel-based method requires far more computation time than the subcrown-based heuristics and even several hours for some Prostate 3D cases. Surprisingly, on average, the subcrown-based heuristics reaches a lower LMSD_{ds} criteria than the voxel-based method, although the difference may hardly be seen in the produced consensus. On those datasets, we were not able to estimate the true minimizer of LMSD_{ds} , due to the high memory resources those computations would require.

Table 3: Mean LMSD_{ds} and computation time for three different heuristics on some datasets

Dataset	Subcrown	Crown	Voxel
MSSEG	16.36 (57.48s)	16.50 (23.41s)	16.36 (20min30s)
Prostate 3D	1.24e-2 (31.5s)	1.26e-2 (5.46s)	NA
Prostate 2D	5.98e-3 (0.29s)	6.22e-3 (0.07s)	6.10e-3 (5.30s)

4.3 Comparison with baseline methods

Comparison of inter-rater variabilities A first set of experiments consist in measuring the impact of the choice of the consensus method when computing a measure of inter-rater variability. More precisely, we compute the average precision, recall, and F1-score between the hard consensus (considered as ground truth) and each rater segmentation. Those metrics have been computed on the MSSEG dataset where there are potentially large disagreements between raters. Table 4 reports those metrics averaged among all lesions of all images, a

lesion corresponding to a connected component of the mask union \mathcal{E}_S . The MV consensus has the highest recall and lowest precision which can be interpreted by a MV consensus smaller than other methods. Conversely, the STAPLE consensus has the largest precision and lowest recall, thus corresponding to a larger size consensus. Regarding terms of F1-score, MV and MACCHIatO methods obtained similar metrics but slightly higher for MACCHIatO-D (0.449).

Table 4: Averaged lesion-wise measures on the MSSEG dataset for all hard consensus methods

Method \ Measure	ML STAPLE	MV	MACCHIatO-J	MACCHIatO-D
Precision	0.976	0.497	0.562	0.570
Recall	0.273	0.817	0.769	0.758
F1-score	0.297	0.437	0.448	0.449

In addition, we also compared the methods on the number of connected components. To do so, we defined each consensus as ground truth and from there computed the average precision, recall, and F1-score of each rater for lesion detection (considering the existence of a non-null intersection with the rater’s segmentation as a sufficient threshold to detect). We performed this experiment on the MSSEG dataset, as it is our only dataset with several connected components per case. Table 5 reports those metrics averaged among all patients. The MV consensus has the highest detection recall and lowest detection precision which can be interpreted by a MV consensus not segmenting some lesions conserved by the other methods. Conversely, the STAPLE consensus has the largest precision and lowest recall, thus corresponding to the presence of lesions rarely segmented by the raters. In terms of F1-score, MV and MACCHIatO methods are close to each other, but it is highest for MACCHIatO-D (0.894).

Table 5: Measures of lesion detection on the MSSEG dataset for all hard consensus methods

Method \ Measure	ML STAPLE	MV	MACCHIatO-J	MACCHIatO-D
Precision	0.994	0.887	0.914	0.931
Recall	0.643	0.967	0.931	0.930
F1-score	0.746	0.892	0.888	0.894

Comparison of consensus areas or volumes In Table 6, we compare the relative size of hard consensus on all datasets, taking the MV consensus as reference. On average, all methods lead to consensus of larger size than MV. For the MACCHIatO methods, the difference with MV consensus is modest on a massive organ (prostate) but significant for small lesions ($>16\%$). The ML STAPLE method generates much larger consensus than MV, especially when dealing with small lesions. Note that for the MSSEG dataset, ML STAPLE is computed on the whole image, thus with a large background size. Finally, the MACCHIatO-D and MACCHIatO-J methods lead to consensus of similar size, without

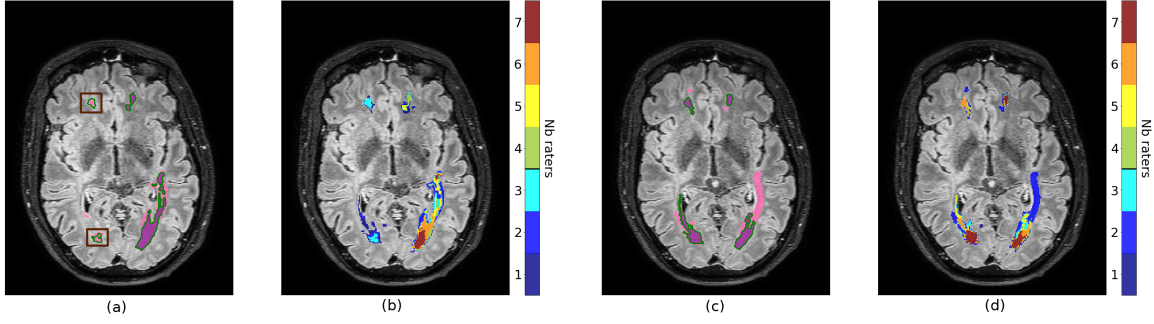


Figure 6: Two consecutive slices of a MSSEG sample on which we applied STAPLE (pink), Majority Voting (purple) and MACCHiatO-TJ (green contour) (a, c), and for each voxel of those slices the number of raters who segmented them (b, d). We can note that some zones (highlighted by brown squares) were selected by soft MACCHiatO-TJ whereas less than the majority of raters segmented them.

any clear order. Table 7 compares the soft area or volumes of the soft consensus (given by $\sum_{n=1}^N \tilde{U}_n$) generated by all methods, taking the mask averaging as reference. Fig. 6 illustrates those soft consensus on the MSSEG dataset. The variation of volumes is smaller for soft consensus than for hard consensus. In general, the MA method produces the smallest volumes, and STAPLE the largest ones. The methods using surrogate Dice or Jaccard distances give similar volumes, although the Soergel and $1SD$ are more diverging on the MSSEG dataset. We also compare the size of the thresholded maps $\tilde{U}_n > 0.5$ which provide similar trends to their soft maps.

For both hard and soft consensus, the largest differences between the different methods are observed on the MSSEG dataset, followed by SCGM-GM.

Table 6: Left : Average size variation on 3D datasets for hard consensus, with the Majority Voting serving as the reference size. Right : percentage of cases where the computed consensus is strictly larger than the MV consensus. Red color indicates that for this setting, all cases are at least of equal size.

Method Dataset	Avg. size variation w.r.t MV			Frequencies of size $> MV $		
	Jaccard	Dice	ML STAPLE	Jaccard	Dice	ML STAPLE
Prostate 3D	+0.4%	+0.6 %	+22%	87.5%	85%	100%
MSSEG	+19%	+16%	+151%	100%	93%	100%
SCGM-SC	+2.36%	+2.30%	+11%	97.5%	97.5%	100%
SCGM-GM	+17%	+15%	+47%	100%	100%	100%

We recorded the cumulative running time for STAPLE and soft MACCHiatO methods to generate a consensus for all structures of our datasets in Table 8. We did not consider MA as it requires far less computation than the other methods. Among the considered algorithms STAPLE is in general the fastest method, being approximately 2-3 times faster

Table 7: Top : Average soft volume variation on 3D datasets for soft consensuses, with the MA serving as the reference. Bottom : Percentage of cases where the obtained consensus has a higher volume than the MA consensus. Red color indicates for the thresholded case that for this setting, all cases are at least of equal size.

Method Dataset	Avg. soft volume variation w.r.t MA				
	TJ	SJ	2SD	1SD	STAPLE
Prostate 3D	+0.4%	+0.1%	+0.1%	+0.7%	+10%
Thresholded	+0.1%	+0.07%	+0.09%	+0.03%	+11%
MSSEG	+4%	+16%	+2%	-3%	+43%
Thresholded	+8%	+37%	+4%	+11%	+68%
SCGM-SC	-0.4%	+0.5%	-0.5%	+0.3%	+4%
Thresholded	+1%	+1.3%	+0.9%	+0.9%	+5.7%
SCGM-GM	+1.2%	+4.4%	+1%	+2.9%	+8.6%
Thresholded	+13%	+16%	+11%	+14%	+19%

Method Dataset	Frequencies of soft volume > MA			
	TJ	SJ	2SD	1SD
Prostate 3D	80%	65%	60%	80%
Thresholded	22.5%	12.5%	7.5%	7.5%
MSSEG	87%	100%	73%	33%
Thresholded	93%	100%	80%	93%
SCGM-SC	10%	52.5%	5%	37.5%
Thresholded	35%	67.5%	25%	27.5%
SCGM-GM	92.5%	95%	92.5%	82.5%
Thresholded	100%	100%	100%	100%

than MACCHIato methods. The exception here is the computation time on SCGM, which always involves small structure sizes and large image sizes.

Table 8: Computation time of continuous methods on all datasets

Method \ Dataset	TJ	SJ	2SD	1SD	STAPLE
Prostate 2D	11.1s	14.6s	7.4s	9.8s	2.3s
Prostate 3D	15m02s	12m52s	9m19s	9m48s	4m17s
MSSEG	14m29s	11m31s	11m42s	11m13s	3m38s
SCGM-SC	16.7s	15.1s	14s	14.3	40.6s
SCGM-GM	14.1s	12.8s	12.4s	13.3s	34.7s

4.4 Entropy of soft consensus

In Figs. 3 and 7 we show examples of soft consensus on the prostate and grey matter datasets. It appears that MACCHIato-SJ and MACCHIato-1SD methods often assign to subcrowns probability values very close to 0 or 1 despite being soft consensus methods. To confirm this behaviour, we compared on all 3D datasets the Shannon entropy $-\sum_n \tilde{U}_n \log \tilde{U}_n - (1 - \tilde{U}_n) \log(1 - \tilde{U}_n)$ obtained by MA and by the four soft MACCHIato methods. Table 9 confirms the strong binary behavior of MACCHIato-SJ and MACCHIato-1SD methods while MACCHIato-TJ and MACCHIato-2SD have a similar spread than mask averaging. Thus, we classify the surrogate distances between two families : the ones associated with low-entropy consensus (Soergel, d_{1SD}), and the ones generating high-entropy consensus (Tanimoto, d_{2SD}).

Table 9: Mean entropy on 3D datasets for soft MACCHIato methods. MA entropy is given as a reference.

Dataset	MA	TJ	SJ	2SD	1SD
Prostate 3D	63850	63658	6928	63799	19361
MSSEG	41295	37377	3805	37720	6107
SCGM-SC	2401	2467	259	2483	305
SCGM-GM	757	736	97	736	118

4.5 Discussion

Experiments confirmed the dependence on background size of the STAPLE method, as shown in Fig. 1a and Appendix A (Tab. 10). We also observed that hard consensus obtained by MACCHIato were generally slightly larger than those obtained by MV, particularly with MACCHIato-J which almost never produces consensus smaller than MV's. This can be explained by the fact that the MACCHIato consensus may include voxels segmented by less than half of the raters (as seen in Figs. 3 and 6). Finally, STAPLE consensus always have a larger size than both MACCHIato and MV. Similar observations can be made on soft consensus but with a smaller difference between methods on soft volumes

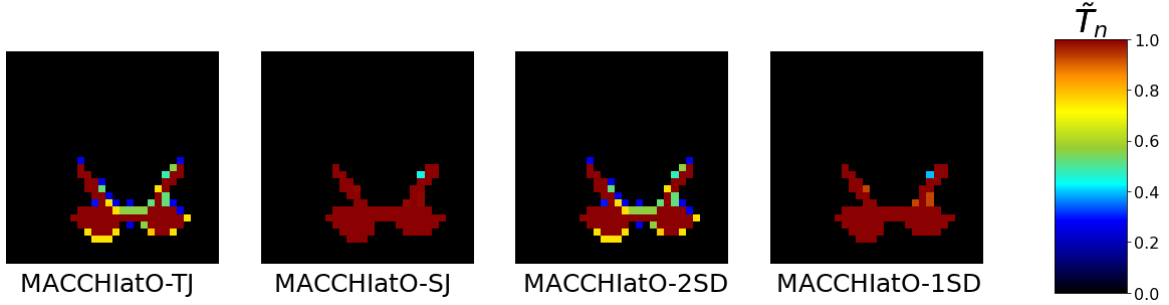


Figure 7: Impact of the choice of the distance on the computed soft MACCHIatO consensus on a SCGM-GM example

compared to hard volumes. The MACCHIatO methods by construction create consensus, independent from the background size, that maximize the local average (soft) squared Dice or Jaccard coefficients between the consensus and rater masks for each connected component. Furthermore, they produce masks that are different from the MV and STAPLE methods and have in general larger volumes than MV consensus and smaller volumes than STAPLE ones. Finally, the MACCHIatO algorithms are in general more computationally expensive than MV or STAPLE algorithms but only to a reasonable extent (about 2 or 3 times more). In this article, we had the deliberate position not to choose between soft and hard consensus. From our perspective, the choice of method should be based on the users' motivations and the downstream task. If the users solely aim to generate a binary mask for visualization purposes or inter-rater variability studies, they can opt for the hard consensus method. However, if they wish to incorporate uncertainty modeling and obtain more refined results, the soft consensus methods would be more suitable.

Similarly, the choice of distances should align with the intended objectives. If users prioritize a solid mathematical foundation for the method, then they may opt for the Jaccard (hard) and Soergel (soft) metrics as, contrary to other used distances, they respect the triangular inequality. Alternatively, the Tanimoto distance can be used for uncertainty assessment, as MACCHIatO-TJ outputs more non-binary values than MACCHIatO-SJ. Users also have the flexibility to use the more commonly employed Dice instead of Jaccard if they prefer. In definitive, we have presented a range of methods within a consistent framework and elaborated on their characteristics. However, the specific configuration is ultimately left to the users based on their individual requirements and preferences.

It can also be noted that the size variation observed on a dataset seems to be correlated with its inter-rater variability, the observed differences being more important on the MSSEG and SCGM-GM dataset than on the others.

In this article, we always considered 8-connexity in 2D cases and 26-connexity in 3D cases, as it performed better in preliminary experiments. However, the use of other neighborhoods (such as the 4-neighborhood in 2D, or the 6 and 18-neighborhood in 3D) could be envisaged. Moreover, we did not consider the case of highly anisotropic images, like in the SCGM dataset where a ratio of anisotropy greater than 10 in the voxel size is encountered. For those cases, it could be considered to apply a 2.5D approach consisting in applying our

method to each slice independently. Comparisons between 2.5D and 3D neighborhoods on SCGM are available in Appendix D.

The proposed method has several limitations. First, we only considered a binary segmentation problem. Extension to multiclass segmentation could be foreseen using for instance the generalization method presented in Crum et al. (2006) and Sudre et al. (2017). Second, the considered distances between binary sets are based on region overlap measures (Dice, Jaccard indices) and discard distances between boundaries such as Hausdorff Distance (HD). Our experiments based on HD were not conclusive.

The reasons for this may be similar to the ones described in Karimi and Salcudean (2019) : instability of the methods to minimize a distance only defined from the largest error, HD sensitivity to outliers, difficulties to optimize it from an optimization point of view. To mitigate those effects, we made some tests using two of the Hausdorff alternatives defined in Karimi and Salcudean (2019) and based respectively on distance maps and erosion, to no avail.

Third, the proposed criteria LMSD_d , weights all raters equally for all connected components, unlike the STAPLE algorithm. It is possible to extend the MACCHIatO framework by attributing weights to raters based on their precision and recall (as those measures are independent of background size), either at the local or global level. Yet, this extension would require additional optimization steps, since the weights depend on the current estimate of the consensus.

Extending the MACCHIatO method to generate consensus from K (soft) probability maps instead of binary segmentations is not straightforward. Indeed, while minimizing the Fréchet variance of Eq. 7 is well-posed, we can no longer restrict its computation to the set \mathcal{E}_S and define subcrowns as optimization blocks. An alternative method that we have explored in our prior work Audelan et al. (2020), is to map probabilities to real values through a link function (e.g. a logit function) and then use robust parametric models (t-distributions) to fuse the probability maps.

5. Conclusion

In this paper, we have shown that the STAPLE method is impacted by the image background size and the choice of prior law. We have also introduced a new background-size independent method to generate a consensus based on Jaccard and Dice-based distances, thus extending the Majority Voting and mean consensus methods. More precisely, the generated masks minimize the average squared Jaccard or Dice distance between the consensus and each rater segmentation. The MACCHIatO algorithms are efficient and provide consistent masks by taking into account local morphological configurations between rater masks. The consensus masks are usually larger than those generated by the majority voting or mask averaging methods but smaller than those issued by STAPLE. Therefore, based on the experiments performed on three datasets, we believe that the hard and soft MACCHIatO algorithms are good alternatives to MV-based and STAPLE-based methods to define consensus segmentation.

Acknowledgments

This work has been supported by the French government, through the 3IA Côte d’Azur Investments and UCA DS4H Investments in the Future project managed by the National Research Agency (ANR) with the reference numbers ANR-19-P3IA-0002 and ANR-17-EURE-0004 and by the Health Data Center of the AP-HP (Assistance Publique-Hôpitaux de Paris). Private data was extracted from the Clinical Data Warehouse of the Greater Paris University Hospitals (Assistance Publique-Hôpitaux de Paris). We thank Julien Castelneau, software Engineer Inria, for his help in the development of MedInria Software (MedInria - Medical image visualization and processing software by Inria <https://med.inria.fr/> - RRID :SCR_001462). The authors are grateful to the OPAL infrastructure from Université Côte d’Azur for providing resources and support. We also thank Alexandre Allera, Malek Ezziane, Anna Luzurier, Raphaëlle Quint and Mehdi Kalai for providing prostate segmentations, Yann Fraboni and Etrit Haxholli for insightful discussions, and Federica Cruciani and Lucia Innocenti for feedback.

This paper is dedicated to the memory of our dear colleague Olivier Commowick who has been very active and innovative in the domain of data fusion.

Ethical Standards

The work follows appropriate ethical standards in conducting research and writing the manuscript, following all applicable laws and regulations regarding treatment of animals or human subjects.

Conflicts of Interest

We declare we do not have conflicts of interest

References

- P. Aljabar, R.A. Heckemann, A. Hammers, J.V. Hajnal, and D. Rueckert. Multi-atlas based segmentation of brain images: Atlas selection and its effect on accuracy. *NeuroImage*, 46(3):726–738, 2009. ISSN 1053-8119. doi: 10.1016/j.neuroimage.2009.02.018.
- Andrew Asman and Bennett Landman. Formulating Spatially Varying Performance in the Statistical Fusion Framework. *Medical Imaging, IEEE Transactions on*, 31:1326–1336, 06 2012. doi: 10.1109/TMI.2012.2190992.
- Andrew J. Asman and Bennett A. Landman. Non-local statistical label fusion for multi-atlas segmentation. *Medical Image Analysis*, 17(2):194–208, 2013. ISSN 1361-8415. doi: 10.1016/j.media.2012.10.002.
- Benoît Audelan, Dimitri Hamzaoui, Sarah Montagne, Raphaële Renard-Penna, and Hervé Delingette. Robust Fusion of Probability Maps. In Anne L. Martel, Purang Abolmaesumi, Danail Stoyanov, Diana Mateus, Maria A. Zuluaga, S. Kevin Zhou, Daniel Racoceanu,

- and Leo Joskowicz, editors, *Medical Image Computing and Computer Assisted Intervention - MICCAI 2020*, pages 259–268, Cham, 2020. Springer International Publishing. ISBN 978-3-030-59719-1.
- Anton S. Becker, Krishna Chaitanya, Khoschy Schawkat, Urs J. Muehlematter, Andreas M. Hötker, Ender Konukoglu, and Olivio F. Donati. Variability of manual segmentation of the prostate in axial t2-weighted mri: A multi-reader study. *European Journal of Radiology*, 121:108716, 2019. ISSN 0720-048X. doi: <https://doi.org/10.1016/j.ejrad.2019.108716>.
- Olivier Commowick, Alireza Akhondi-Asl, and Simon K. Warfield. Estimating A Reference Standard Segmentation with Spatially Varying Performance Parameters: Local MAP STAPLE. *IEEE Transactions on Medical Imaging*, 31(8):1593–1606, August 2012. doi: 10.1109/TMI.2012.2197406.
- Olivier Commowick, Audrey Istace, Michael Kain, Baptiste Laurent, Florent Leray, Mathieu Simon, Sorina Camarasu Pop, Pascal Girard, Roxana Ameli, Jean-Christophe Ferré, Anne Kerbrat, Thomas Tourdias, Frédéric Cervenansky, Tristan Glatard, Jeremy Beaumont, Senan Doyle, Florence Forbes, Jesse Knight, April Khademi, Amirreza Mahbod, Chunliang Wang, Richard Mckinley, Franca Wagner, John Muschelli, Elizabeth Sweeney, Eloy Roura, Xavier Llado, Michel Santos, Wellington P Santos, Abel G Silva-Filho, Xavier Tomas-Fernandez, Hélène Urien, Isabelle Bloch, Sergi Valverde, Mariano Cabezas, Francisco Javier Vera-Olmos, Norberto Malpica, Charles R G Guttmann, Sandra Vukusic, Gilles Edan, Michel Dojat, Martin Styner, Simon K. Warfield, François Cotton, and Christian Barillot. Objective Evaluation of Multiple Sclerosis Lesion Segmentation using a Data Management and Processing Infrastructure. *Scientific Reports*, 8(1):13650, December 2018. doi: 10.1038/s41598-018-31911-7.
- William Crum, Oscar Camara, and Derek Hill. Generalized Overlap Measures for Evaluation and Validation in Medical Image Analysis. *IEEE transactions on medical imaging*, 25: 1451–61, 12 2006. doi: 10.1109/TMI.2006.880587.
- Bin Dai, Shilin Ding, and Grace Wahba. Multivariate Bernoulli distribution. *Bernoulli*, 19 (4):1465–1483, 2013.
- Anne-Sophie Dewalle-Vignion, Nacim Betrouni, Clio Baillet, and Maximilien Vermandel. Is STAPLE algorithm confident to assess segmentation methods in PET imaging? *Physics in Medicine and Biology*, 11 2015. doi: 10.1088/0031-9155/60/24/9473.
- Michel Marie Deza and Elena Deza. Distances and Similarities in Data Analysis. In *Encyclopedia of Distances*, pages 327–345, Berlin, Heidelberg, 2016. Springer Berlin Heidelberg. ISBN 978-3-662-52844-0. doi: 10.1007/978-3-662-52844-0_17.
- Alonso Gragera and Vorapong Suppakitpaisarn. Relaxed triangle inequality ratio of the Sørensen–Dice and Tversky indexes. *Theoretical Computer Science*, 718:37–45, 2018. ISSN 0304-3975. doi: <https://doi.org/10.1016/j.tcs.2017.01.004>. URL <https://www.sciencedirect.com/science/article/pii/S0304397517300361>. WALCOM (Workshop on Algorithms and Computation).

- Dimitri Hamzaoui, Sarah Montagne, Raphaële Renard-Penna, Nicholas Ayache, and Hervé Delingette. Morphologically-aware jaccard-based iterative optimization (mojito) for consensus segmentation. In Carole H. Sudre, Christian F. Baumgartner, Adrian Dalca, Chen Qin, Ryutaro Tanno, Koen Van Leemput, and William M. Wells III, editors, *Uncertainty for Safe Utilization of Machine Learning in Medical Imaging*, pages 3–13, Cham, 2022. Springer Nature Switzerland. ISBN 978-3-031-16749-2.
- Fabian Isensee, Paul F. Jaeger, Simon A. A. Kohl, Jens Petersen, and Klaus H. Maier-Hein. nnU-Net: a self-configuring method for deep learning-based biomedical image segmentation. *Nature Methods*, 18:203–211, 2021. doi: 10.1038/s41592-020-01008-z.
- Wei Ji, Shuang Yu, Junde Wu, Kai Ma, Cheng Bian, Qi Bi, Jingjing Li, Hanruo Liu, Li Cheng, and Yefeng Zheng. Learning calibrated medical image segmentation via multi-rater agreement modeling. In *Proceedings of the IEEE/CVF Conference on Computer Vision and Pattern Recognition (CVPR)*, pages 12341–12351, June 2021.
- Davood Karimi and Septimiu E Salcudean. Reducing the Hausdorff Distance in Medical Image Segmentation with Convolutional Neural Networks. *IEEE Transactions on medical imaging*, 39(2):499–513, 2019.
- Sven Kosub. A note on the triangle inequality for the Jaccard distance. *Pattern Recognition Letters*, 120:36–38, 2019. ISSN 0167-8655.
- Dieter Kraft. A software package for sequential quadratic programming. Technical Report DFVLR-FB 88-28, DLR German Aerospace Center – Institute for Flight Mechanics, Koln, Germany, 1988.
- Andrew R. Leach and Valerie J. Gillet. Similarity Methods. In *An Introduction To Chemoinformatics*, pages 99–117, Dordrecht, 2007. Springer Netherlands. ISBN 978-1-4020-6291-9. doi: 10.1007/978-1-4020-6291-9_5.
- Bradley Lowekamp, David Chen, Luis Ibanez, and Daniel Blezek. The Design of SimpleITK. *Frontiers in Neuroinformatics*, 7, 2013. doi: 10.3389/fninf.2013.00045.
- Jun Ma, Jianan Chen, Matthew Ng, Rui Huang, Yu Li, Chen Li, Xiaoping Yang, and Anne L. Martel. Loss odyssey in medical image segmentation. *Medical Image Analysis*, 71:102035, 2021. ISSN 1361-8415. doi: <https://doi.org/10.1016/j.media.2021.102035>. URL <https://www.sciencedirect.com/science/article/pii/S1361841521000815>.
- Sarah Montagne, Dimitri Hamzaoui, Alexandre Allera, Malek Ezziiane, Anna Luzurier, Raphaëlle Quint, Mehdi Kalai, Nicholas Ayache, Hervé Delingette, and Raphaëlle Renard Penna. Challenge of prostate MRI segmentation on T2-weighted images: inter-observer variability and impact of prostate morphology. *Insights into Imaging*, 12(1), June 2021. doi: 10.1186/s13244-021-01010-9.
- Ferran Prados, John Ashburner, Claudia Blaiotta, Tom Brosch, Julio Carballido-Gamio, Manuel Jorge Cardoso, Benjamin N. Conrad, Esha Datta, Gergely Dávid, Benjamin De Leener, Sara M. Dupont, Patrick Freund, Claudia A.M. Gandini Wheeler-Kingshott, Francesco Grussu, Roland Henry, Bennett A. Landman, Emil Ljungberg, Bailey Lyttle,

- Sebastien Ourselin, Nico Papinutto, Salvatore Saporito, Regina Schlaeger, Seth A. Smith, Paul Summers, Roger Tam, Marios C. Yiannakas, Alyssa Zhu, and Julien Cohen-Adad. Spinal cord grey matter segmentation challenge. *NeuroImage*, 152:312–329, 2017. ISSN 1053-8119. doi: <https://doi.org/10.1016/j.neuroimage.2017.03.010>. URL <https://www.sciencedirect.com/science/article/pii/S1053811917302185>.
- Torsten Rohlfing and Calvin R. Maurer. Shape-Based Averaging. *IEEE Transactions on Image Processing*, 16(1):153–161, 2007. doi: 10.1109/TIP.2006.884936.
- Mert R. Sabuncu, B. T. Thomas Yeo, Koen Van Leemput, Bruce Fischl, and Polina Golland. A generative model for image segmentation based on label fusion. *IEEE Transactions on Medical Imaging*, 29(10):1714–1729, 2010. doi: 10.1109/TMI.2010.2050897.
- H Späth. The Minisum Location Problem for the Jaccard Metric. *Operations-Research-Spektrum*, 3:91–94, 1981.
- Carole H. Sudre, Wenqi Li, Tom Vercauteren, Sebastien Ourselin, and M. Jorge Cardoso. Generalised Dice Overlap as a Deep Learning Loss Function for Highly Unbalanced Segmentations. In M. Jorge Cardoso, Tal Arbel, Gustavo Carneiro, Tanveer Syeda-Mahmood, João Manuel R.S. Tavares, Mehdi Moradi, Andrew Bradley, Hayit Greenspan, João Paulo Papa, Anant Madabhushi, Jacinto C. Nascimento, Jaime S. Cardoso, Vasileios Belagiannis, and Zhi Lu, editors, *Deep Learning in Medical Image Analysis and Multimodal Learning for Clinical Decision Support*, pages 240–248, Cham, 2017. Springer International Publishing.
- Pauli Virtanen, Ralf Gommers, Travis E. Oliphant, Matt Haberland, Tyler Reddy, David Cournapeau, Evgeni Burovski, Pearu Peterson, Warren Weckesser, Jonathan Bright, Stéfan J. van der Walt, Matthew Brett, Joshua Wilson, K. Jarrod Millman, Nikolay Mayorov, Andrew R. J. Nelson, Eric Jones, Robert Kern, Eric Larson, C J Carey, İlhan Polat, Yu Feng, Eric W. Moore, Jake VanderPlas, Denis Laxalde, Josef Perktold, Robert Cimrman, Ian Henriksen, E. A. Quintero, Charles R. Harris, Anne M. Archibald, Antônio H. Ribeiro, Fabian Pedregosa, Paul van Mulbregt, and SciPy 1.0 Contributors. SciPy 1.0: Fundamental Algorithms for Scientific Computing in Python. *Nature Methods*, 17:261–272, 2020. doi: 10.1038/s41592-019-0686-2.
- S.K. Warfield, K.H. Zou, and W.M. Wells. Simultaneous truth and performance level estimation (STAPLE): an algorithm for the validation of image segmentation. *IEEE Transactions on Medical Imaging*, 23(7):903–921, 2004. doi: 10.1109/TMI.2004.828354.
- Peter Willett, John M. Barnard, and Geoffrey M. Downs. Chemical Similarity Searching. *Journal of Chemical Information and Computer Sciences*, 38(6):983–996, 1998. doi: 10.1021/ci9800211.
- Le Zhang, Ryutaro Tanno, Mou-Cheng Xu, Chen Jin, Joseph Jacob, Olga Ciccarrelli, Frederik Barkhof, and Daniel Alexander. Disentangling Human Error from Ground Truth in Segmentation of Medical Images. In H. Larochelle, M. Ranzato, R. Hadsell, M.F. Balcan, and H. Lin, editors, *Advances in Neural Information Processing Systems*, volume 33, pages 15750–15762. Curran Associates, Inc., 2020.

Appendix A. Influence of background size in STAPLE

We can see that by definition u_n is impacted by the value of w_n and, through TN_k , by the background size $BS = |\{n|\forall k, S_n^k = 0\}|$ (i.e. the number of voxels that no rater segmented). In the following subsections we will characterize the dependence of the produced consensus to those parameters.

A.1 STAPLE dependence on background size at fixed foreground

By definition, when the background size increases TN_k also increases whereas TP_k, FP_k and FN_k remain constants. So, $q_k \rightarrow 1$ when $BS \rightarrow \infty$ and we can write

$$\begin{aligned} \text{logit}(u_n) &\sim \text{logit}(w_n) + \sum_{k, S_n^k=1} (\ln(p_k) - \ln(1 - \frac{TN_k}{TN_k + FP_k})) + \sum_{k, S_n^k=0} \ln(1 - p_k) \\ &\sim \text{logit}(w_n) + \sum_{k, S_n^k=1} (\ln(p_k) - \ln(\frac{FP_k}{N - B_k})) + \sum_{k, S_n^k=0} \ln(1 - p_k) \\ &\sim \text{logit}(w_n) + \sum_{k, S_n^k=1} (\ln(N - B_k) + \ln(\frac{p_k}{FP_k})) + \sum_{k, S_n^k=0} \ln(1 - p_k) \end{aligned}$$

with $B_k = TP_k + FN_k$.

A.2 Impact of the consensus prior w_n on the limit

In Warfield et al. (2004), they proposed to set w_n as a spatially uniform value $w_n = w$ where w is either a constant (typically $w = 0.5$) or defined as the average occurrence ratio ($w = \frac{1}{NK} \sum_{n,k} S_n^k$). We further consider more general priors of the form $w = \frac{A}{N^\alpha}$, with A a constant independent of the image size BS , thus having $\text{logit}(w_n) = -\ln(\frac{N^\alpha - A}{A})$.

From there, we can write

$$\begin{aligned} \lim_{BS \rightarrow \infty} \text{logit}(u_n) &= -\ln(\frac{N^\alpha - A}{A}) + \sum_{k, S_n^k=1} \ln(N - B_k) + \sum_{k, S_n^k=1} \ln(\frac{p_k}{FP_k}) + \sum_{k, S_n^k=0} \ln(1 - p_k) \\ &= \sum_{k, S_n^k=1} \ln(N - B_k) - \ln(N^\alpha - A) + \ln(A) + \sum_{k, S_n^k=1} \ln(\frac{p_k}{FP_k}) + \sum_{k, S_n^k=0} \ln(1 - p_k) \\ &\sim \sum_{k, S_n^k=1} \ln(N) - \alpha \ln(N) + \ln(A) + \sum_{k, S_n^k=1} \ln(\frac{p_k}{FP_k}) + \sum_{k, S_n^k=0} \ln(1 - p_k) \end{aligned}$$

And

$$\lim_{BS \rightarrow \infty} u_n = \frac{1}{1 + (\frac{1}{A} \prod_k \frac{FP_k^{S_n^k}}{p_k^{S_n^k(1-p_k)^{1-S_n^k}}}) N^{\alpha - \sum_k S_n^k}}$$

Table 10: Mean soft consensus entropy and volume comparisons on Prostate 3D between STAPLE on the full image (Full size STAPLE) and on a bounded box surrounding the organ (Focused STAPLE).

Dataset	Measure	Full size STAPLE	Focused STAPLE
Prostate 3D	Entropy	2019	10992
	Size	300534	285329
SCGM-SC	Entropy	74	269
	Size	11406	11275
SCGM-GM	Entropy	71	118
	Size	1854	1838

Appendix B. Proof of Majority Voting as a Fréchet Mean

With $S^1, S^2, \dots, S^K \in \{0, 1\}^N$ binary segmentation maps and T their Fréchet mean with regards to the function $\sqrt{A \Delta B} = \sqrt{|(A \cup B) \setminus (A \cap B)|}$, we have

$$\begin{aligned}
T &= \arg \min_{M \in \{0,1\}^N} \sum_k (\sqrt{|(S^k \cup M) \setminus (S^k \cap M)|})^2 = \arg \min_{M \in \{0,1\}^N} \sum_k (\sqrt{|(S^k \cup M) \setminus (S^k \cap M)|})^2 \\
&= \arg \min_{M \in \{0,1\}^N} \sum_k (\sum_n (S_n^k + M_n - S_n^k M_n) - S_n^k M_n) = \arg \min_{M \in \{0,1\}^N} \sum_{k,n} S_n^{k^2} + M_n^2 - 2S_n^k M_n \\
&= \arg \min_{M \in \{0,1\}^N} \sum_n (\sum_k (S_n^k - M_n)^2) = (\delta(\sum_k S_n^k > \frac{K}{2}))_n (\text{the Majority Voting consensus}).
\end{aligned}$$

Appendix C. Inter-rater variability

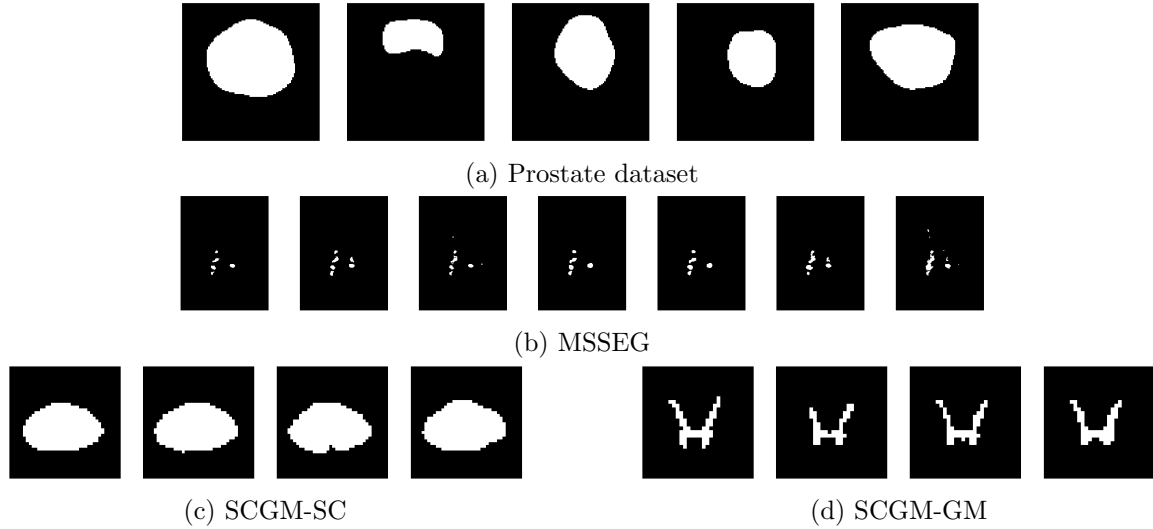


Figure 8: Example of the inter-rater variability between the raters for the different datasets.

Appendix D. Comparison between 2.5D and 3D neighborhoods

Table 11: Size comparisons for hard MACCHIAtOs between the 2.5D and 3D neighborhood on SCGM-SC (top) and SCGM-GM (bottom)

Method	Avg. size variation w.r.t MV		Direct size comparisons	
	3D	2.5D	$ 3D > 2.5D $	$ 3D < 2.5D $
Jaccard	+2.37%	+1.66%	32.5%	65%
Dice	+2.3%	+1.6%	37.5%	55%

(a) SCGM-SC

Method	Avg. size variation w.r.t MV		Direct size comparisons	
	3D	2.5D	$ 3D > 2.5D $	$ 3D < 2.5D $
Jaccard	+16.9%	+15.8%	77.5%	15%
Dice	+14.7%	+14.9%	67.5%	27.5%

(b) SCGM-GM

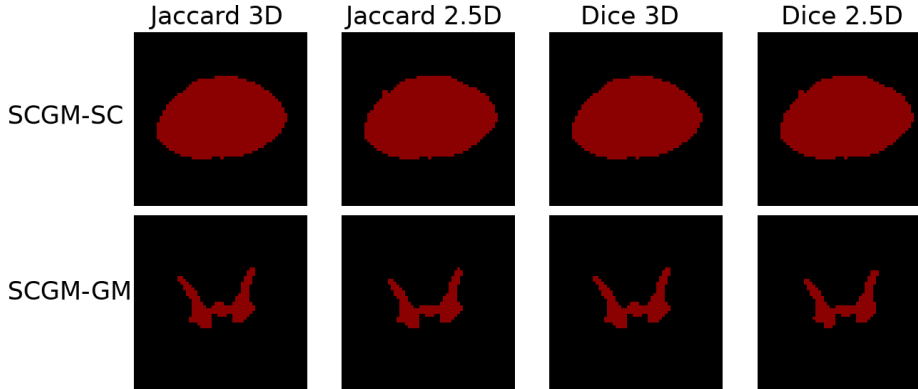


Figure 9: Examples of hard consensus on SCGM with 2.5D and 3D neighborhoods.